

Morphological manipulation of the nonlinear optical response of ZnO thin films grown by thermal evaporation

This content has been downloaded from IOPscience. Please scroll down to see the full text.

2014 Mater. Res. Express 1 046201

(<http://iopscience.iop.org/2053-1591/1/4/046201>)

View the [table of contents for this issue](#), or go to the [journal homepage](#) for more

Download details:

IP Address: 14.139.69.191

This content was downloaded on 20/11/2014 at 04:03

Please note that [terms and conditions apply](#).

Morphological manipulation of the nonlinear optical response of ZnO thin films grown by thermal evaporation

Ummar Pasha Shaik¹, P Ajay Kumar¹, M Ghanashyam Krishna^{1,2} and S Venugopal Rao

¹ Advanced Center of Research in High Energy Materials (ACRHEM), University of Hyderabad, Prof. C.R. Rao Road, Hyderabad 500046, India

² School of Physics, University of Hyderabad, Prof. C.R. Rao Road, Hyderabad 500046, India
E-mail: mgksp@uohyd.ernet.in and soma_venu@yahoo.com

Received 26 July 2014, revised 26 September 2014

Accepted for publication 23 October 2014

Published 19 November 2014

Materials Research Express **1** (2014) 046201

[doi:10.1088/2053-1591/1/4/046201](https://doi.org/10.1088/2053-1591/1/4/046201)

Abstract

ZnO thin films with different micro-/nano-structured morphologies have been fabricated using thermal evaporation technique. The micro-/nano-structures ranged from dense grains to nanorods and nanowires. The fabricated films were characterized using x-ray diffraction and field emission scanning electron microscopy (FE-SEM) techniques for determining their crystalline behavior and evaluating their morphology, respectively. Photoluminescence (PL) studies revealed two emission peaks in these films, one in the UV region due to exciton emission and the other in the visible spectral region due to Zn or Oxygen vacancies/defects. The effect of these different micro-/nano-structures on the third-order nonlinear optical (NLO) response has been scrutinized using the Z-scan technique with femtosecond (fs), MHz and picosecond (ps), kHz pulses at a wavelength of 800 nm. Various NLO coefficients such as two-photon absorption (β), nonlinear refractive index (n_2), $\text{Re}[\chi^{(3)}]$, $\text{Im}[\chi^{(3)}]$ and $\chi^{(3)}$ were evaluated. The obtained $\chi^{(3)}$ values were $\sim 10^{-7}$ e.s.u. in the fs regime and $\sim 10^{-10}$ e.s.u. in the ps regime. Optical limiting studies of these films were also performed and limiting thresholds were estimated to be $15\text{--}130 \mu\text{J cm}^{-2}$ in the fs regime while in ps regime the corresponding values were $1\text{--}3 \text{ J cm}^{-2}$. The NLO data clearly designates strong third-order nonlinearities in these ZnO thin films with possible applications in photonics.

Keywords: ZnO nanostructures, Z-scan, luminescence, optical properties

1. Introduction

Zinc Oxide (ZnO) is one of the most efficient II–VI semiconductors because of its large optical band gap, high linear refractive index and electrical properties which are responsible for a variety of applications in electronics, acousto-optic devices, photonic devices, sensors, solar cells, and optoelectronic devices [1–4]. ZnO is a direct band gap (3.37 eV) semiconductor with large exciton binding energy (60 meV), which is much higher than that of ZnSe and GaN, leading to room temperature UV laser emission. ZnO also finds applications in UV laser diodes, and several other varieties of applications such as in exciton related photonic devices [5–8]. The advantage of wide band gap incorporates high-temperature/high-power operation, lower noise generation, higher breakdown voltages and ability to sustain large electric fields. ZnO nanowires (NWs) and nanorods in structured films have fascinating applications in nano-lasers, random lasers, biosensors, UV-LEDs, self-lighting photodynamic therapy for treatment of cancer, and innovative nano-devices to name a few [9–15]. Optical nonlinearities in semiconductors are of particular interest due to the possibility of application in optical switches, optical limiters, and all-optical signal processing [16]. It has been demonstrated over the years that nanostructuring of materials leads to significant enhancement in nonlinear optical (NLO) behavior [17]. Several groups have proposed that composite materials in thin film form would exhibit enhanced NLO behavior [18, 19]. The higher order NLO susceptibilities are known to be a sum of the contributions from the bulk and surface and it is well documented that surface roughness plays an important role in determining the NLO response of metals [20]. Zn–ZnO based composites have recently shown promise with the demonstration of enhanced emission in UV and visible region [21].

NLO properties of a variety of ZnO films and nanostructures grown using different techniques and growth conditions have recently been reported [7–9, 11, 22–38]. Chan *et al* [8] studied ZnO thin films and observed two-photon absorption (2PA, β) values of 10^{-6} – 10^{-7} cm W⁻¹ in the wavelength range of 390–420 nm using 82 MHz, 100 fs pulses. Han *et al* [9] have reported ZnO thin film data with β of 10^{-6} – 10^{-7} cm W⁻¹ at 790 nm using 76 MHz, ~140 fs pulses. Irimpan *et al* [23–26] have reported NLO properties of nanostructured ZnO thin films with 2PA coefficients of $\sim 10^{-4}$ – 10^{-9} cm W⁻¹ and $\chi^{(3)}$ of $\sim 10^{-6}$ – 10^{-10} e.s.u. with ns pulses. Ouyang *et al* [31] studied the 2PA and optical limiting properties of graphene/ZnO composites in organic glasses and reported a NLO coefficient (α_2) of 1530 cm GW⁻¹. Lee *et al* [35] synthesized ZnO nanorods with different rod diameters (50, 110, 240 nm) and investigated their fs NLO properties and time response of the nonlinearity. However, most of the studies were performed using (a) single (ns/ps/fs) pulse excitation (b) MHz, fs pulse excitation and very few of them attempted investigating exhaustive structure–property relationship. Furthermore, with fs pulses and MHz excitation one expects thermal contribution to the observed nonlinearities without clear contribution of electronic nonlinearity. The objective of current work was to fabricate ZnO films with different micro-/nano-structures and investigate the NLO response keeping crystallographic details the same in all cases. We have performed both femtosecond (fs) NLO studies with MHz/kHz repetition rate in conjunction with picosecond (ps) NLO studies with kHz repetition rate for all the fabricated films. It is demonstrated that the NLO response of ZnO films can be controlled by manipulating their microstructures. Our earlier studies on such ZnO films investigated the wettability, Raman, Photoluminescence (PL) properties in detail [15, 21].

2. Experimental details

ZnO films were grown by thermal evaporation technique on borosilicate glass (BSG) substrates by four different annealing approaches. ZnO films were prepared by two different routes to achieve different micro-/nano-structures. In the first process, deposition of ZnO film was achieved using zinc oxide powder as the source material followed by annealing at 150 °C in air (sample named as ZnO-film; ZnO1). The second process involved thermal oxidation of metallic Zn films in air or oxygen atmosphere at 500 °C. Three different types of thermal oxidation routes were followed: 1) annealing of Zn film at 500 °C maintaining a heating rate of 5 °C min⁻¹ followed by soaking time of 30 min at the same temperature (sample named as ZnO-Air; ZnO2) 2), the same as 1 except the annealing is carried out in an oxygen rich atmosphere (sample named as ZnO-oxygen; ZnO3) 3) Zn film was rapid annealed at 500 °C in air atmosphere. i.e., initially the furnace was heated to 500 °C at the rate of 10 °C min⁻¹ and then the sample was loaded and maintained at the same temperature for 30 min followed by natural cooling in normal furnace atmosphere (sample named as ZnO4). Thicknesses of these films were measured using a surface profilometer (XP 100 of Ambios Technology, USA). Post annealing, the thicknesses of films were ~250 nm, ~980 nm, ~670 nm and ~1500 nm for ZnO1, ZnO2, ZnO3, and ZnO4, respectively. The crystal structures of ZnO films were characterized by a high resolution x-ray diffractometer (XRD) using Cu K α radiation of wavelength 0.15408 nm. The effect of annealing routes on surface morphology was investigated by field emission scanning electron microscopy (FE-SEM) (Carl Zeiss Model Ultra 55).

Optical absorption of the films was measured in the 200–2500 nm spectral range using a UV-vis-NIR spectrophotometer (JASCO V-570). The Raman spectra were recorded in air using a Nd:YAG laser at 532 nm in the back scattering geometry in a CRM spectrometer equipped with a confocal microscope and 100X objective with a CCD detector (model alpha 300 of WiTec, Germany). The PL spectra were recorded in air in the same spectrometer using a 355 nm diode laser with ~7 mW input power in reflection configuration and 40X UV objectives with a CCD detector (WiTec, Germany). NLO characterization was accomplished using the standard Z-scan technique [39]. In the fs regime, a Ti: sapphire oscillator (Chameleon Ultra II, Coherent) producing ~140 fs pulses with a repetition 80 MHz at 800 nm was used. The sample was scanned along the Z-direction through the focus of a 100 mm focal length lens. The input beam was spatially filtered to obtain a pure Gaussian profile in the far field. The sample was placed on a 10 μ m resolution translation stage and data was collected manually using the detector (Field-Max). The transmitted intensity was recorded as a function of the sample position. The beam waist (ω_0) estimated at the focus was ~25 μ m with a corresponding Rayleigh range of ~2.54 mm. In the ps regime, studies were performed by using Ti: sapphire amplifier delivering ~2 ps, 1 kHz pulses at 800 nm. The amplifier was seeded with ~15 fs pulses from an oscillator (MICRA, Coherent, 1 W, 80 MHz, 800 nm). The average power from amplifier was ~2 W. The laser beam was focused by a 200 mm focal length lens. The output transmittance was recorded by using a photodiode in combination with a lock-in amplifier. Complete details of the ps experiments have been reported in our earlier works [40–43]. The NLO studies were performed on all the samples with linear transmittance of ~60–75% at 800 nm. All the closed aperture scans were performed at lower peak intensities so as to avoid any contribution from higher order nonlinear effects (the value of $\Delta\phi$ estimated in all the cases was < π). The experiments were repeated more than once and the average nonlinear optical coefficients were retrieved from the theoretical fits to experimental data.

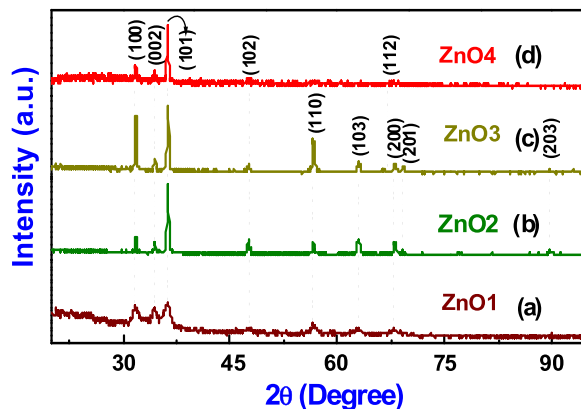


Figure 1. XRD pattern of thin films of (a) ZnO1 (b) ZnO2 (c) ZnO3 and (d) ZnO4.

3. Results and discussion

The XRD data of ZnO1, ZnO2, ZnO3, and ZnO4 are shown in figure 1. The diffraction peaks of all samples exactly coincided with that of hexagonal ZnO structure and the peaks were indexed according to JCPDS No. 89-1397. We did not observe any significant Zn residue from the XRD patterns of ZnO2, ZnO3 and ZnO4 [figures 1(b)–(d)], which confirmed that there was a complete phase transition from hexagonal Zn (as deposited) to hexagonal ZnO at 500 °C annealing temperature [15].

The hexagonal ZnO unit cell parameters were calculated from the XRD patterns and were independent of oxidation history of the samples. The calculated unit cell parameters were, $a = 3.2 \pm 0.2 \text{ \AA}$ and $c = 5.2 \pm 0.2 \text{ \AA}$. The average crystallite sizes were calculated from FWHM of ZnO peaks using Scherrer's formula [44] and the obtained value was $36 \pm 2 \text{ nm}$ for the three films of ZnO2, ZnO3, and ZnO4 and independent of different oxidation approaches used. However, ZnO1 had a crystallite size of $8 \pm 2 \text{ nm}$. The lower value of the crystallite size in the case of ZnO1 can be attributed to the lower annealing temperature as well as the lower thickness of this film.

The morphology of ZnO1 is displayed in figure 2(a). The SEM data revealed a dense microstructure with flakes emerging out of the surface. Closer examination revealed that there were pores in the film which were randomly distributed. Morphology of ZnO2 (depicted in figure 2(b)) also resulted in dense microstructure but there was evidence for formation of aggregates on the surface which rendered the surface rough. The microstructure of ZnO3 (data presented in figure 2(c)) depicts formation of micro/nanorods that grew along the plane of the film surface. However, the most drastic change occurred in the microstructure of ZnO4, shown in figure 2(d). There was transformation into nanowires with diameters of $\sim 15\text{--}100 \text{ nm}$ and lengths extending to a few μm emerging from the film surface. From the high resolution images presented in figures 2(e)–(h) it is evident that the annealing route had a significant effect on the surface morphology of ZnO films. The microstructures ranged from dense films to slightly porous microstructures, micro/nano rods and nanowires. Hence, these samples provided good examples for investigating the effect of differing microstructures on NLO properties of resulting ZnO surfaces.

To know the growth direction of obtained ZnO nanowires, ZnO4 sample was examined under TEM. Figure 3(a) shows the bright field TEM image of ZnO nanowire selected from

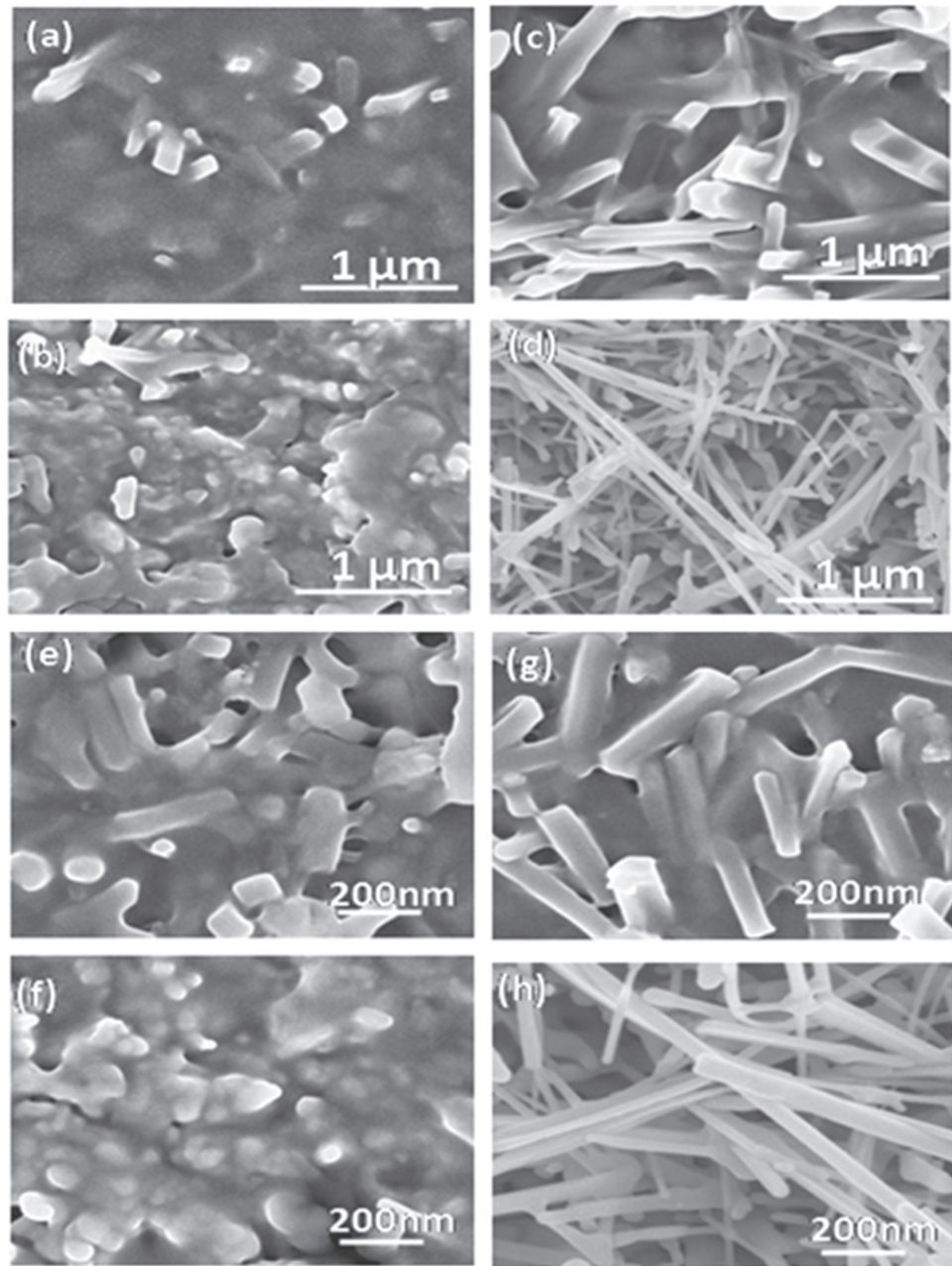


Figure 2. FE-SEM images of (a), (e) ZnO1 (b), (f) ZnO2 (c), (g) ZnO3 (d), (h) ZnO4. (a)-(d) are in $1\text{ }\mu\text{m}$ scale and (e)-(h) are in 200 nm scale.

ZnO4 sample. The bright field image shows the nanowire of diameter 30 nm and length 800 nm. Selected area electron diffraction (SAED) pattern of the ZnO nanowire shows that the Wurtzite structure of ZnO was formed (inset of figure 3(a)). Figure 3(b) shows the HRTEM image of the same single ZnO nanowire presented in the bright field image of figure 3(a). From the fast Fourier transform (FFT) (inset of figure 3(b)) analysis of the high resolution TEM (HRTEM) images, the d spacing between lattice planes was calculated as 0.28 nm, indicating that the ZnO nanowires were grown in $[1\ 0\ -1\ 0]$ direction. Our results are in good agreement with the previous reported results [45–47].

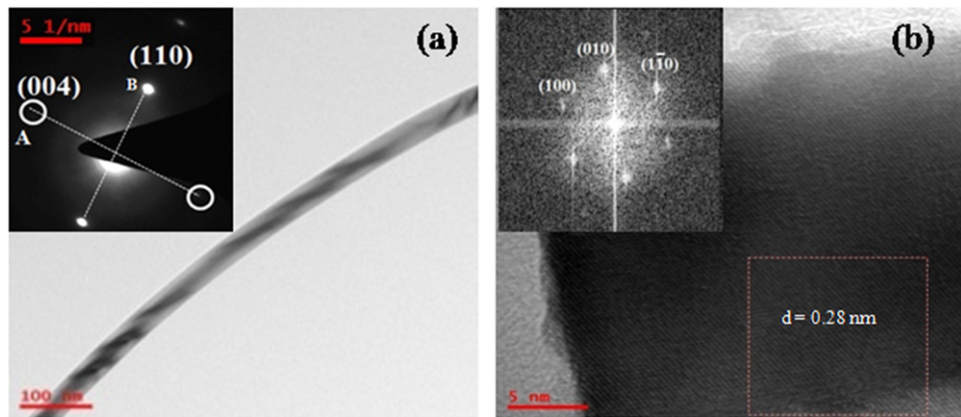


Figure 3. (a) Bright field image, inset SAED and (b) HRTEM image, inset FFT of single ZnO nanowire of ZnO4 sample.

The absorption coefficient α is related to incident photon energy ' $h\nu$ ' by the Tauc's relation [48] $(\alpha h\nu) = (\text{const}) (h\nu - E_g)^n$. $n = 1/2$ and $n = 2$ for the direct and indirect transitions in crystalline semiconductors, respectively. Optical band gap E_g was calculated by linear extrapolating the plot of $(\alpha h\nu)^{1/n}$ versus $h\nu$ and finding the intersection with abscissa [49]. The optical band gap values (E_g) of ZnO thin films were calculated from absorption spectra presented in figure 4(a). The E_g values of ZnO1, ZnO2, ZnO3, and ZnO4 determined from the Tauc plots shown in figures 4(b) to (e) were 3.69 eV, 3.53 eV, 3.50 eV, and 3.15 eV, respectively. It is to be noted that the large difference in thickness of ZnO1 (250 nm), ZnO2 (980 nm) and ZnO3 (670 nm) samples has a very negligible effect on the band gap. The lower value of the optical band gap, 3.15 eV, of the ZnO4 sample (which consists of nanowires) is due to the partial oxidation of the sample leading to oxygen non-stoichiometry. However, in all the cases there is clear evidence for the presence of defect states in the range of 2.5–3.1 eV range (see figures 4(b)–(e)) which manifests itself as the UV peak in the PL spectra (see discussion below) and the 2PA data (see discussion below).

PL spectra of ZnO1, ZnO2, ZnO3 and ZnO4 thin films excited at a photon energy of 3.49 eV (355 nm) are presented in figure 5. It is well established that bulk and thin film ZnO exhibit three PL peaks, a UV near band-edge emission peak near 380 nm, a green emission near 510 nm and a red emission in the vicinity of 650 nm [50–52]. In our earlier work on similar films, the dominant near band edge emission peak in 370–380 nm spectral region has been ascribed to exciton–exciton scattering process from the $n=1$ state to the exciton continuum state (P-line) while the broad emission observed near 550 nm is assigned to oxygen vacancies (V_o) [21]. The broad green-yellow band near 505 nm is due to deep level emissions in green region, which is ascribed to oxygen vacancies, zinc interstitials or zinc vacancies [53]. In the present study we have observed UV near band edge emission peak in the 383–394 nm range and visible emission in the 489–543 nm range from the films. These two peaks are frequently originating luminescent peaks reported in all ZnO samples. Thus, the results of the present study are in excellent agreement with earlier reports on thin films and bulk ZnO [21, 52, 54–58]. It should be noted that the appearance of sharp, narrow UV emission splitting into two is an indication of better crystallinity and good quality of ZnO nanowires growth [21, 59] which is in excellent agreement with XRD and FE-SEM results. We repeated the PL measurements for

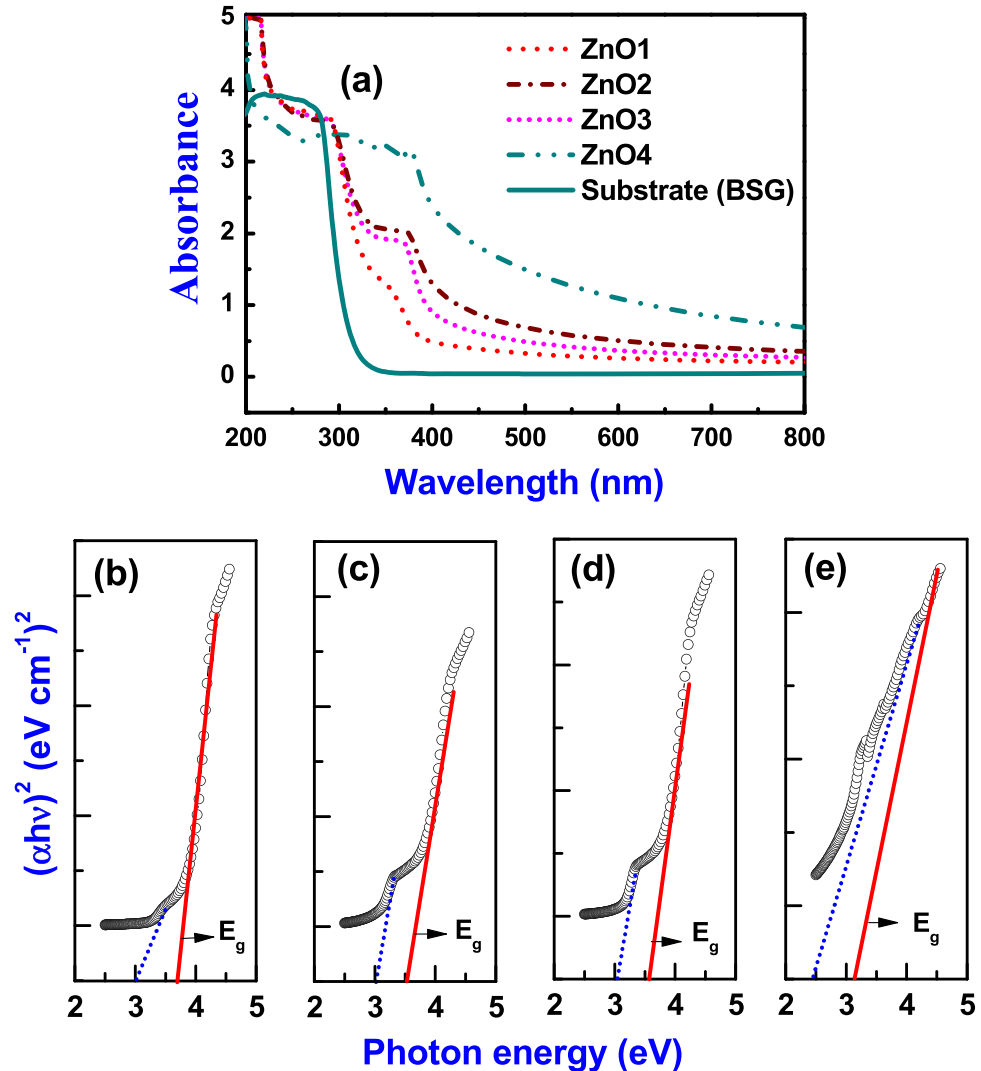


Figure 4. (a) Absorption spectra of ZnO1, ZnO2, ZnO3, and ZnO4 thin films. Substrate absorption spectrum (solid line) is also included. (b)–(e) Tauc plots for ZnO1–ZnO4; red (solid line) indicates the band gap, blue (dotted) line represents the presence of defect states.

ZnO1 and ZnO4 samples after four months and did not find any significant changes in the recorded spectrum. This suggested that the samples were stable and devoid of any aging effects.

Wurtzite ZnO belongs to C6V (P63mc) space group for which the possible vibrational modes [60] are

$$U_{\text{opt}} = A1 + 2B1 + E1 + 2E2$$

where A1, E1, and E2 are Raman active and B1 is Raman forbidden. The room temperature Raman spectra of ZnO thin films are shown in figure 6. The first order optical modes of ZnO at 380.8 cm^{-1} and 437.5 cm^{-1} are assigned to the A1 (transverse optical (TO)) and E₂ high, optical phonons, respectively [60–62]. The most intense peak at 437.5 cm^{-1} is the characteristic peak of ZnO Wurtzite phase and can be attributed to the E₂ high mode. The peaks at 299.8 cm^{-1} , 329.7 cm^{-1} , 550.6 cm^{-1} and 674.6 cm^{-1} have earlier been observed in bulk ZnO by other

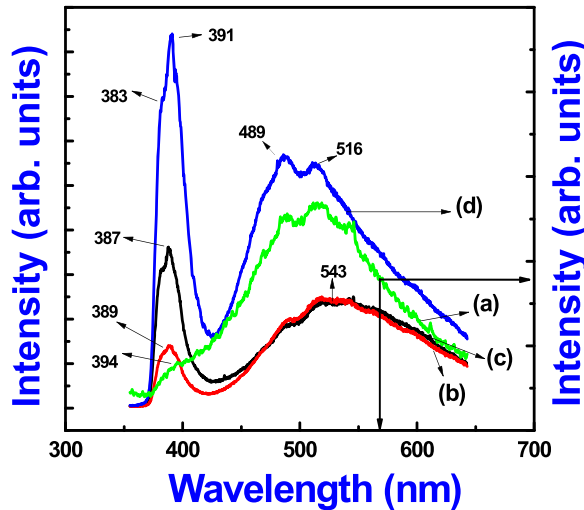


Figure 5. PL spectra of (a) ZnO1 (b) ZnO2 (c) ZnO3 and (d) ZnO4 thin films excited with above band gap energy (355 nm) of ZnO.

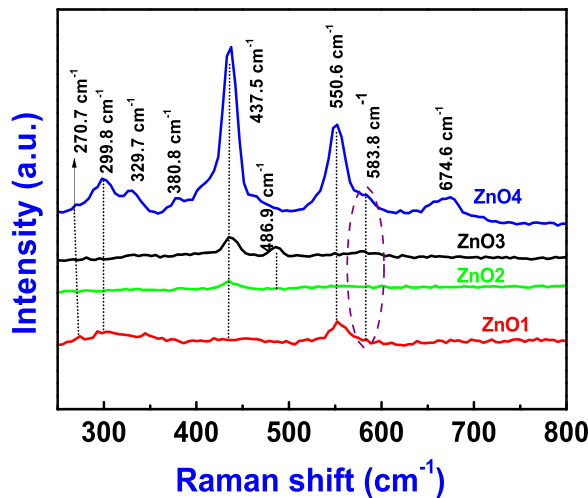


Figure 6. Raman spectra of ZnO1, ZnO2, ZnO3 and ZnO4.

workers and assigned to B_1 low, E_{2H} - E_{2L} , B_1 high and transverse acoustic (TA) + longitudinal acoustic (LA) modes, respectively [56, 63, 64]. The peak at 486.9 cm^{-1} has been attributed to surface optical phonons from earlier works [62]. The peak at 270.7 cm^{-1} is the laser plasma line [60] while the peak at 583.8 cm^{-1} assigned to E_1 (LO) has been inferred to arise from the formation of defects of oxygen vacancies [60, 65, 66].

Evidently both the Raman and PL spectra demonstrated the presence of oxygen related defects/vacancies. The corresponding energy level diagram inferred from these spectra is displayed in figure 7. From this energy level diagram and the calculated band gaps, it is expected that all the films would exhibit two-photon absorption (2PA) in the nonlinear absorption studies performed with ps and fs pulses.

In the fs regime, Z-scan data was recorded for ZnO1, ZnO2, and ZnO3 at 800 nm. The signatures are shown in figure 8 and corresponding NLO coefficients obtained from the fits to

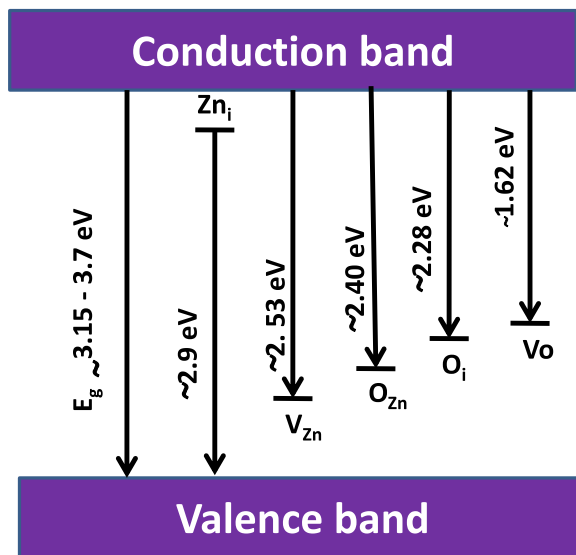


Figure 7. Typical energy level diagram of ZnO films studied. Zn_i and O_i are the Zn and Oxygen interstitials, V_{Zn} and V_o are the Zn and Oxygen vacancies.

experimental data are presented in table 1. As stated earlier (based on the PL and Raman data) 2PA was observed for all films. We obtained β values of $0.99\text{--}1.3 \times 10^{-4} \text{ cm W}^{-1}$ for data recorded with peak intensities of $0.2\text{--}0.3 \text{ GW cm}^{-2}$. The values of nonlinear refractive index, n_2 , were $\sim 14\text{--}27 \times 10^{-10} \text{ cm}^2 \text{ W}^{-1}$ obtained with peak intensity of $\sim 0.034 \text{ GW cm}^{-2}$. These values represent one of the highest reported values for ZnO nanostructures in literature. There could be contributions from various sources to the nonlinear refractive index including electronic, molecular, electrostriction, and excited state absorption population. In the fs (MHz) regime ZnO1 and ZnO3 depicted negative nonlinearity (self-de-focusing type) as evident from the peak-valley signature while ZnO2 depicted positive nonlinearity (self-focusing type) as evident from the valley-peak signature. The peak valley distance ($\sim 4.4 \text{ mm}$) was $\sim 1.7 \times Z_0$ in the case of ZnO1 and ZnO3 which confirms the presence of Kerr (purely electronic) type of nonlinearity. Earlier studies suggest bound electrons being responsible for negative n_2 in ZnO single crystals [29]. In the case of ZnO2 there could be contribution from thermal or excited state population [29, 30]. The reason for this discrepancy requires further detailed investigation. The Z-scan data for ZnO1 was also examined using a 1 kHz optical chopper (original repetition rate was 80 MHz) and the data is shown in figure 9. One should note that these are not the regular 1 kHz pulses obtained from fs amplifiers. We observed that there were no significant changes in the order of magnitude of NLO coefficients.

In the ps regime, Z-scan data was recorded for ZnO1, ZnO2, ZnO3 and ZnO4 at 800 nm and the data is presented in figure 10. We again observed 2PA behavior in all the films. β values retrieved from the fits were $\sim 1.15\text{--}9.5 \times 10^{-8} \text{ cm W}^{-1}$ achieved with peak intensities of $\sim 100\text{--}152 \text{ GW cm}^{-2}$ while the n_2 values were $6.8\text{--}39 \times 10^{-13} \text{ cm}^2 \text{ W}^{-1}$ achieved with a peak intensity of $\sim 28 \text{ GW cm}^{-2}$. Interestingly ZnO1 and ZnO3 demonstrated positive nonlinearity (self-de-focusing, valley-peak signature) while ZnO2 and ZnO4 exhibited negative nonlinearity (self-focusing, peak-valley signature). The peak-valley distance was $\sim 1.7 \times Z_0$ in the case of ZnO2 and ZnO4 which confirms the presence of Kerr (purely electronic) type of nonlinearity. In the case of ZnO3 and ZnO4 the switchover of sign could possibly be related to their band gaps

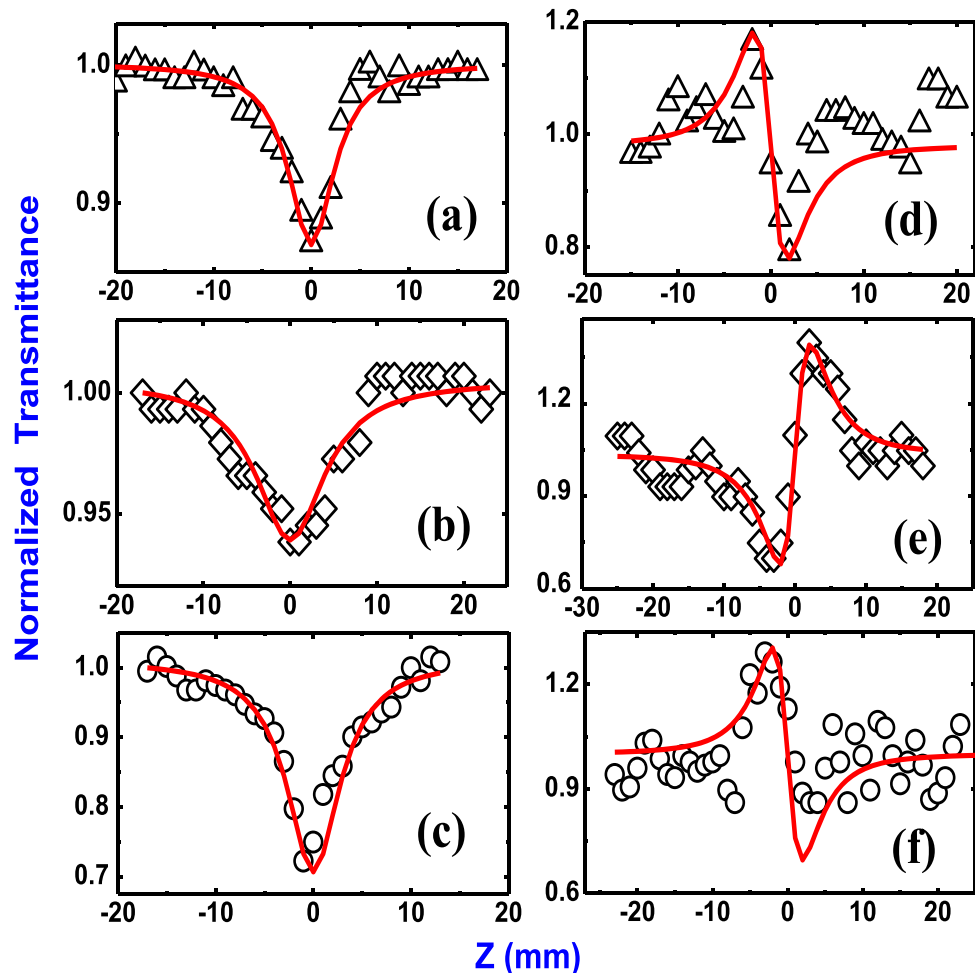


Figure 8. The fs open aperture Z-scan data of (a) ZnO1 (open triangles) (b) ZnO2 (open diamonds) (c) ZnO3 (open circles). Peak intensity used was $\sim 0.21 \text{ GW cm}^{-2}$. Closed aperture Z-scan data of (d) ZnO1 (open triangles) (e) ZnO2 (open diamonds) (f) ZnO3 (open circles). Peak intensity used was $\sim 0.034 \text{ GW cm}^{-2}$. Solid lines (red) in all graphs represent theoretical fits.

and/or excited state population resulting from 2PA. The excitation was with 1.55 eV photons in all the cases. Earlier studies [35] indicated that the local field enhancements through size- and structure-dependent interfacial interactions influence the magnitude of n_2 . The Z-scan data was fitted using standard equations reported in literature [67]. The NLO coefficients retrieved from ps data are summarized in table 2. All the coefficients were estimated with $\pm 15\%$ uncertainty arising from errors in beam waist measurements and calibration of filters. Tables 1 and 2 also present some of the recently reported NLO coefficients of ZnO films and composites by various groups. With ps (kHz excitation) and fs (kHz excitation) excitation ZnO1 depicted the strongest NLO properties amongst all four samples [including β , n_2 and $\chi^{(3)}$].

A survey of literature shows that the values of β and n_2 are strongly dependent on the processing technique leading to a large scatter in the values of these coefficients. This is also a consequence of the fact that microstructural evolution of thin films is, in general, process dependent. Therefore, not surprisingly, the values of β and n_2 for our samples (ZnO1–ZnO4)

Table 1. Estimated NLO coefficients β , n_2 , $\chi^{(3)}$ of ZnO films in the fs regime. Negative sign indicates negative nonlinearity. Some of the recent works are also highlighted.

Sample	β (cm MW ⁻¹)	n_2 (cm ² GW ⁻¹)	Im $\chi^{(3)} \times 10^{-7}$ (e. s.u.)	Re $\chi^{(3)} \times 10^{-7}$ (e. s.u.)	Total $\chi^{(3)} \times 10^{-7}$ (e. s.u.)	Reference
ZnO1 fs MHz pulses	99.0	-2.70	0.55	-2.43	2.49	This work
ZnO2 fs MHz pulses	12.5	1.40	0.07	1.21	1.21	This work
ZnO3 fs MHz pulses	130	-1.74	0.72	-1.51	1.67	This work
ZnO1 fs, kHz pulses	175	-3.70	0.96	-3.20	3.30	This work
ZnO nanorods fs, MHz pulses	-0.6–5.6	0.056–0.31	—	—	—	[35]
ZnO films fs, MHz pulses	$120\text{--}1100 \times 10^{-3}$	—	—	—	—	[9]
ZnO films fs, MHz pulses	$91\text{--}681 \times 10^{-3}$	$1.35\text{--}2.65 \times 10^{-2}$	—	—	—	[68]
ZnO nanoholes fs, MHz pulses	180×10^{-3}	—	—	—	—	[27]
ZnO/graphene ns pulses	1.56	—	—	—	—	[31]

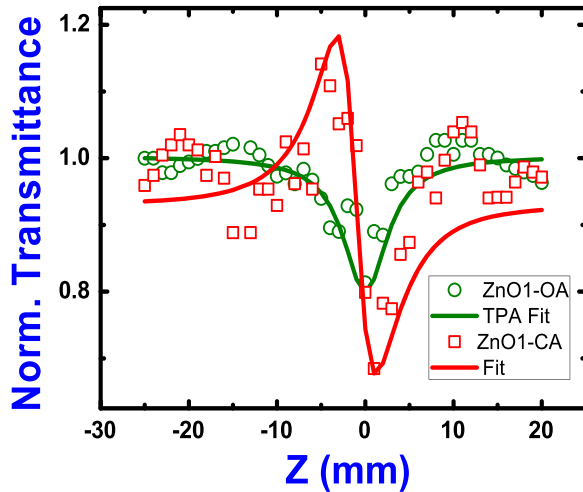


Figure 9. Open aperture data of ZnO1 using 1 kHz chopper (open circles) recorded at peak intensity 0.21 GW cm^{-2} . Solid line (green) represents the 2PA theoretical fit. Closed aperture data of ZnO1 (open squares) recorded at peak intensity of 0.034 GW cm^{-2} . Solid line (red) represents the theoretical fit.

are slightly different to that of the values reported earlier [68]. For example, Lin *et al* [68] studied fs NLO absorption of ZnO thin films grown by laser molecular beam epitaxy and obtained β values of 3000 cm GW^{-1} at 390 nm (or 3 cm MW^{-1}) which was much larger than that of ZnO bulk measured at 532 nm . In contrast, Lee *et al* [35] synthesized vertically aligned ZnO nanorods with different rod diameters (50 nm , 110 nm , 240 nm) and investigated their fs (MHz) NLO properties. They obtained NLO coefficients (β) with magnitudes of $2.91 \times 10^{-6} \text{ cm W}^{-1}$ to $5.61 \times 10^{-6} \text{ cm W}^{-1}$ (i.e. $2.91\text{--}5.61 \text{ cm MW}^{-1}$) at 815 nm . They argue that the high 2PA values may have originated from the large residual absorption at the fundamental and TPA wavelengths and the band-edge local field enhancement due to surface trapped states. They further convey that 2PA-induced thermal nonlinearity could not be fully excluded because of the large absorption at TPA wavelength. In our case too we observe residual absorption at two photon wavelength of 400 nm (Z-scan excitation was at 800 nm). They also reported n_2 values of $0.92\text{--}3.11 \times 10^{-10} \text{ cm}^2 \text{ W}^{-1}$ (i.e. $0.092\text{--}0.311 \text{ cm}^2 \text{ GW}^{-1}$) whereas we observed values in the range of $1.4\text{--}3.7 \text{ cm}^2 \text{ GW}^{-1}$ in our case. However, in their case the rod diameters (vertically aligned) were 50 nm , 110 nm , and 240 nm , whereas in our case the films morphology was completely different. Lee *et al* [35] further summarize that the geometric arrangement of nanostructures strongly varies with the sample thickness and is one of the crucial factors contributing to the observed overall optical nonlinearity, confirming our observation of morphology dependent NLO properties.

Porosity is the property of materials which affects the nonlinear optical response at nanoscale. Earlier studies have indicated that nanoporous Si [69], aluminum oxide nanostructures [70] exhibited large $\chi^{(3)}$ values depending on the pore structure, size, and density. In the case of our samples ZnO1 had well sorted pores, compared to others, probably resulting in a higher $\chi^{(3)}$ for ZnO1. The porosity was highest in ZnO1 films, which leads to the inference that largest $\chi^{(3)}$ value observed for ZnO1 in ps/fs measurements is, possibly, a consequence of its denser microstructure. Similar results were obtained in porous Al oxide nanostructures [70] wherein they demonstrated that the local electric field enhancement was due

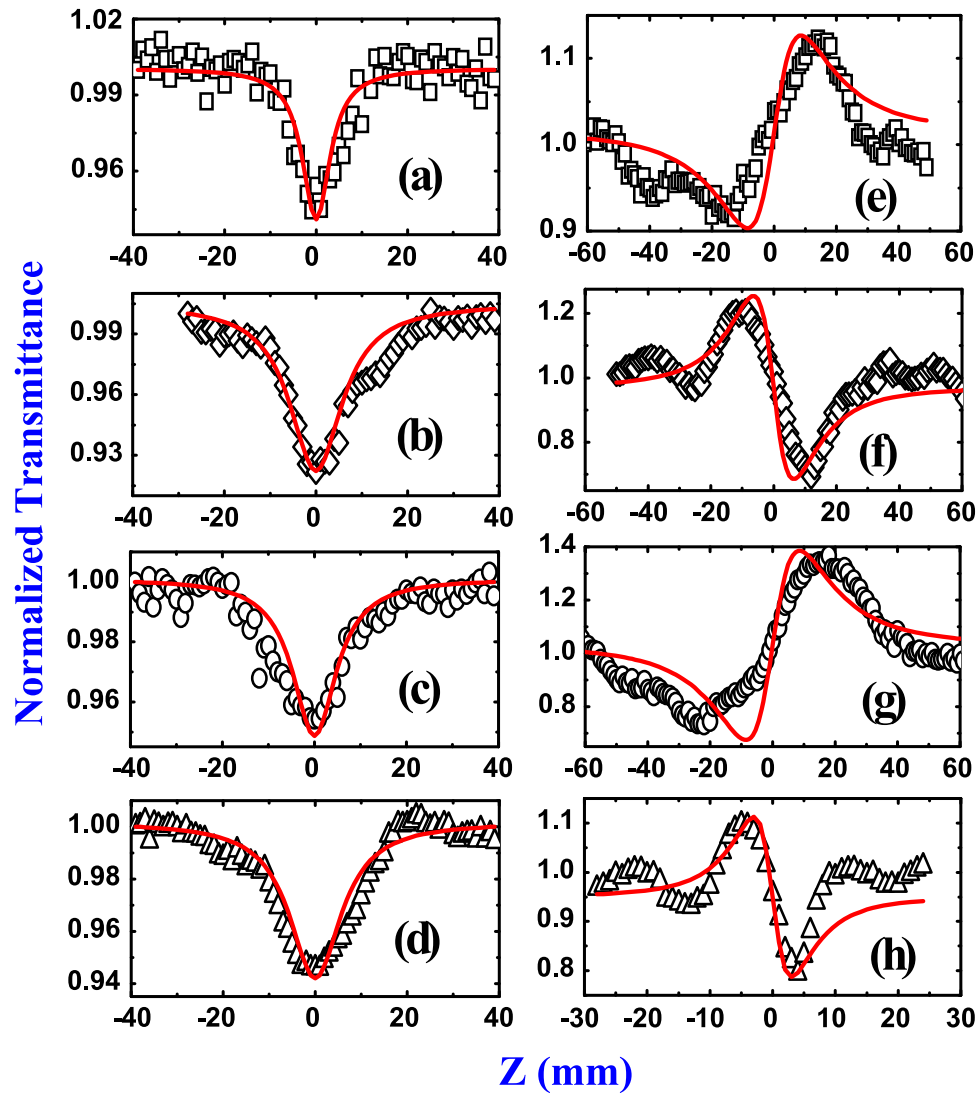


Figure 10. Open aperture Z-scan data of (a) ZnO1 (open squares) at $\sim 100 \text{ GW cm}^{-2}$ (b) ZnO2 (open diamonds) at $\sim 119 \text{ GW cm}^{-2}$ (c) ZnO3 (open circles) recorded at $\sim 144 \text{ GW cm}^{-2}$ (d) ZnO4 (open triangles) at $\sim 152 \text{ GW cm}^{-2}$. Closed aperture Z-scan data of (e) ZnO1 (open squares) (f) ZnO2 (open diamonds) (g) ZnO3 (open circles) (h) ZnO4 (open triangles). Peak intensity used was $\sim 28 \text{ GW cm}^{-2}$. Solid lines (red) in all graphs represent the theoretical fit.

to pore size, pore shape, and surface state effects which in turn enhanced the optical nonlinearity [69]. Han *et al* [9] reported β values of 1.1 cm MW^{-1} for ZnO films annealed at $950\text{--}1050^\circ\text{C}$ and attributed the increased nonlinearity due to the interfacial state enhancement. Trejo *et al* [30] prepared nanostructured ZnO thin solid films by electro deposition of hydrothermal sol-gel solutions and obtained a β value of 4750 cm GW^{-1} but measured at 532 nm and using 180 ps pulses (as against a value of 95 cm GW^{-1} in our case measured at 800 nm and $\sim 2 \text{ ps}$ pulses). The higher value obtained in their case can be attributed to (a) different wavelength and (b) longer duration pulses. The $\chi^{(3)}$ values obtained in the present studies (10^{-7} esu) are similar to that that of $\chi^{(3)}$ values of ZnO microcrystallite thin films [71] studied near the excitonic

Table 2. Estimated NLO coefficients β , n_2 , $\chi^{(3)}$ of ZnO films in the ps regime. Negative sign indicates negative nonlinearity. Some of the recent works are also highlighted.

Sample	β (cm GW $^{-1}$)	n_2 (cm 2 TW $^{-1}$)	Im $\chi^{(3)} \times 10^{-10}$ (e.s.u.)	Re $\chi^{(3)} \times 10^{-10}$ (e.s.u.)	Total $\chi^{(3)} \times 10^{-10}$ (e.s.u.)	Reference
ZnO1 ps, 1 kHz	95.0	3.9	0.530	3.38	3.43	This work
ZnO2 ps, 1 kHz	30.0	-2.2	0.160	-1.89	1.90	This work
ZnO3 ps, 1 kHz	19.5	3.0	0.110	2.59	2.60	This work
ZnO4 ps, 1 kHz	11.5	-0.7	0.064	-0.60	0.60	This work
ZnO-PS ns pulses	0.082–0.281	0.43–1.33	—	—	$5.71\text{--}14 \times 10^{-5}$	[34]
ZnO films ps pulses	-4.75×10^3	7.1×10^{-3}	—	—	0.0123	[30]
ZnO films ns pulses	2.9–103.7 $\times 10^3$	—	—	—	$2.3\text{--}13.4 \times 10^4$	[25]
ZnO nanocones ns pulses	18, 4.6	—	—	—	—	[36]

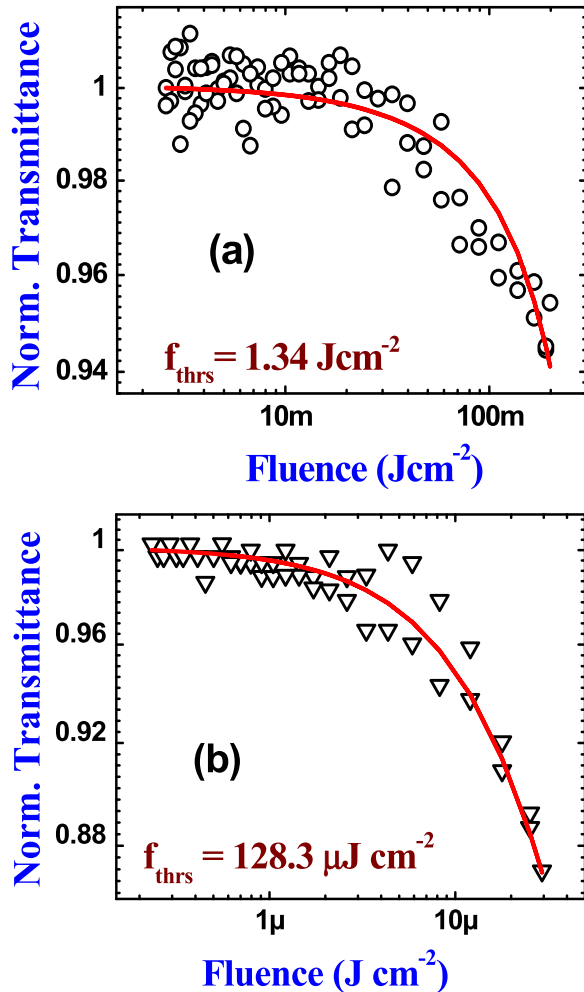


Figure 11. (a) Optical limiting data of ZnO1 (open circles) using ~ 2 ps pulses. Solid line (red) represents the theoretical fit, (b) optical limiting data of ZnO1 (open triangles) using ~ 140 fs pulses. Solid line (red) represents the theoretical fit.

resonance at various temperatures using fs (MHz pulses) degenerate four-wave-mixing technique. Further detailed studies are necessary to exactly identify the mechanism for superior nonlinearities in our case. The values of β and n_2 for pure ZnO thin films measured with fs MHz pulse excitation were $\sim 10^{-6} \text{ cm W}^{-1}$ and $\sim 10^{-11} \text{ cm}^2 \text{ W}^{-1}$, respectively [35]. The values of β and n_2 for bulk ZnO measured using 25 ps, 532 nm excitation were found to be $\sim 4.2 \text{ cm GW}^{-1}$ and $\sim 9 \times 10^{-15} \text{ cm}^2 \text{ W}^{-1}$, respectively [28, 29]. The NLO coefficients β and n_2 of NLO crystals such as KDP and BBO are $\sim 0.9 \text{ cm GW}^{-1}$ and $5-6 \times 10^{-16} \text{ cm}^2 \text{ W}^{-1}$ [72, 73].

Optical limiting (OL) behavior [32, 33] of ZnO thin films in the fs and ps time domains was evaluated and the data is presented in figures 11(a) and (b), respectively. OL threshold values in fs domain were estimated to be $15-130 \mu\text{J cm}^{-2}$, while in ps regime the values were $1-3 \text{ J cm}^{-2}$. Such small limiting threshold values in the fs regime could find practical applications in OL devices. Though many earlier OL studies on pure ZnO films and composites were confined to the ns regime it also imperative to identify materials for OL in the ultrafast (ps/fs) time domain since the detectors/sensors are usually equally prone to laser induced damage

with those pulses associated with large peak intensities. In the fs case the threshold for OL was lower since the magnitude of nonlinearities was large due to thermal contribution. In the ps regime the measurements were performed with kHz pulses and, therefore, the thermal contribution could be negligible.

We have also evaluated the contribution of thermal effects [68] for data recorded with MHz repetition rate. Thermo-optical nonlinearity is an important parameter while calculating the nonlinear index of refraction. In particular, thermo-optic contribution is added by non-local nonlinearity while using ultra short laser pulses. For some materials this contribution becomes significant. It depends on the thermal characteristic time and thermo-optic coefficient. In the first case contribution is significant, if thermal characteristic time τ_c is longer than the time period of the laser. Thermal characteristic time τ_c was calculated using the parameters of beam waist (ω_o), density (ρ), specific heat (c_p), and thermal conductivity (k) [68]

$$\tau_c = \frac{\omega_o^2 \rho c_p}{4k}. \quad (1)$$

The estimated τ_c was $\sim 8.3 \times 10^{-6}$ s for the fs data. The thermo-optic coefficient values for ZnO1, ZnO2, and ZnO3 in the fs regime were calculated using the relation

$$\Delta n_0 = \frac{\alpha F_0}{2\rho c_v} \frac{dn}{dT}. \quad (2)$$

F_0 is the fluence, ρ is the density, c_v is the specific heat, and $\frac{1}{2}$ denotes the fluence averaging factor. Thermo-optic coefficient $\left[\frac{dn}{dT} \right]$ values estimated were (a) ZnO1: 2.14×10^{-4} K $^{-1}$ (b) ZnO2: 2.41×10^{-4} K $^{-1}$ (c) ZnO3: 2.01×10^{-4} K $^{-1}$. In the ps regime we performed the measurements with 1 kHz pulses (1 ms time between consecutive pulses) and, therefore, we expect minimal thermal contributions to the observed nonlinearity and it predominantly has electronic contributions.

Our future studies will focus on (a) recording the spectral dependence of the nonlinearities in the ps regime, (b) understanding the excited state dynamics in these thin films using ps/fs degenerate and non-degenerate pump-probe studies [40, 74, 75] and (c) estimating the figures of merit for NLO application over the entire visible spectral range using ps/fs kHz pulses.

4. Conclusions

NLO characterization in the fs and ps regimes has been performed on ZnO thin films fabricated with different morphologies. The micro-/nano-structures were characterized using XRD (crystalline behavior) and FE-SEM (morphology). All the films exhibited 2PA at 800 nm in both the regimes with magnitudes of $\sim 10^{-4}$ cm W $^{-1}$, $\sim 10^{-8}$ cm W $^{-1}$ in fs, ps regimes, respectively. The n_2 values were $\sim 10^{-9}$ cm 2 W $^{-1}$ in ps and $\sim 10^{-12}$ cm 2 W $^{-1}$ in fs regimes. Third order nonlinearity [$\chi^{(3)}$] values were also estimated. Very low limiting threshold values ($15\text{--}130 \mu\text{J cm}^{-2}$) were recorded with fs pulses. It is demonstrated that NLO response of ZnO films can be controlled by manipulating their microstructures.

Acknowledgments

SVR acknowledges the financial support from DRDO. PAK acknowledges the support of Mr Krishna Podagatlapalli and Mr Syed Hamad during NLO studies. UPS acknowledges support of Dr M A Mohiddon during PL, Raman measurements.

References

- [1] Yan R, Gargas D and Yang P 2009 *Nat. Photon.* **3** 569
- [2] Özgür Ü, Alivov Y I, Liu C, Teke A, Reschikov M A, Doğan S, Avrutin V, Cho S-J and Morkoç H 2005 *J. Appl. Phys.* **98** 041301
- [3] Panda D and Tseng T-Y 2013 *J. Mater. Sci.* **48** 6849
- [4] Dhara S and Giri P K 2013 *Rev. Nanosci. Nanotechnol.* **2** 1
- [5] Ou P-C, Lin J-H, Chang C-A, Liu W-R and Hsieh W-F 2010 *J. Phys. D: Appl. Phys.* **43** 495103
- [6] Tang Z K, Wong G K L, Yu P, Kawasaki M and Ohtomo A 1998 *Appl. Phys. Lett.* **72** 3270
- [7] Das S K, Biswas M, Byrne D, Bock M, McGlynn E, Breusing M and Grunwald R 2010 *J. Appl. Phys.* **108** 043107
- [8] Chan Y-P, Lin J-H, Hsu C-C and Hsieh W-F 2008 *Opt. Express* **16** 19900
- [9] Han Y B, Han J B, Ding S, Chen D J and Wang Q Q 2005 *Opt. Express* **13** 9211
- [10] Gurav K V *et al* 2014 *Sensors Actuators B* **190** 439
- [11] Nagaraja K K, Pramodini S, Poornesh P and Nagaraja H S 2013 *J. Phys. D: Appl. Phys.* **46** 055106
- [12] Thareja R K and Mitra A 2000 *Appl. Phys. B* **71** 181
- [13] Ou P-C, Liu W-R, Ton H-J, Lin J-H and Hsieh W-F 2011 *J. Appl. Phys.* **109** 013102
- [14] Wang K, Zhou J, Yuan L, Tao Y, Chen J, Lu P and Wang Z L 2012 *Nano. Lett.* **12** 833
- [15] Shaik U P, Kshirsagar S, Krishna M G, Tewari S P, Purkayastha D D and Madhurima V 2012 *Mater. Lett.* **75** 51
- [16] Fainman Y, Ma J and Lee S H 1993 *Mater. Sci. Rep.* **9** 53
- [17] Ray P C 2010 *Chem. Rev.* **110** 5332
- [18] Boyd R W, Gehr R J, Fischer G L and Sipe J E 1996 *Pure Appl. Opt.* **5** 505
- [19] Beecroft L L and Ober C K 1997 *Chem. Mater.* **9** 1302
- [20] Poliakov E Y, Markel V A and Shalaev V M 1998 *Phys. Rev. B* **57** 14901
- [21] Kshirsagar S, Shaik U P, Krishna M G and Tewari S P 2013 *J. Lumin.* **136** 26
- [22] Johnson J C, Yan H, Schaller R D, Petersen P B, Yang P and Saykally R J 2002 *Nano. Lett.* **2** 279
- [23] Irimpan L, Deepthy A, Krishnan B, Kukreja L M, Nampoori V P N and Radhakrishnan P 2008 *Opt. Commun.* **281** 2938
- [24] Irimpan L, Deepthy A, Krishnan B, Kukreja L M, Nampoori V P N and Radhakrishnan P 2008 *Appl. Phys. B* **90** 547
- [25] Irimpan L, Nampoori V P N, Radhakrishnan P, Krishnan B and Deepthy A 2008 *J. Appl. Phys.* **103** 033118
- [26] Irimpan L, Ambika D, Kumar V, Nampoori V P N and Radhakrishnan P 2008 *J. Appl. Phys.* **104** 033105
- [27] Zhang L-C, Yang G, Wang K, Fu M, Wang Y, Long H and Lu P-X 2013 *Opt. Commun.* **291** 395
- [28] Zhang X J, Ji W and Tang S H 1997 *J. Opt. Soc. Am. B* **14** 1951
- [29] Zhang X, Fang H, Tang S and Ji W 1997 *Appl. Phys. B* **65** 549
- [30] Trejo-Valdez M, Torres C T-, Chacon J H C-, Armenta G A G-, Gil C I G- and Khomenko A V 2013 *Opt. Laser Technol.* **49** 75
- [31] Ouyang Q-Y, Xu Z, Lei Z, Dong H, Yu H, Qi L, Li C and Chen Y 2014 *Carbon* **67** 214
- [32] Jamal R K, Suhail A M, Hussein M T and Khashi H J 2012 *Int. J. Thin Film Sci. Technol.* **1** 61
- [33] Haripadman P C, Kavitha M K, John H, Krishnan B and Gopinath P 2012 *Appl. Phys. Lett.* **101** 071103
- [34] Jeeju P P, Jayalaxmi S, Chandrasekharan K and Sudheesh P 2012 *Opt. Commun.* **285** 5433

- [35] Lee H W, Lee K M, Lee S, Koh K H, Park J-Y, Kim K and Rotermund F 2007 *Chem. Phys. Lett.* **447** 86
- [36] Haripadman P C, John H, Philip R and Gopinath P 2014 *Opt. Lett.* **39** 474
- [37] Vinodkumar R, Lethy K J, Arunkumar P R, Krishnan R R, Pillai N V, Pillai V P M and Philip R 2010 *Mater. Chem. Phys.* **121** 406
- [38] Prakash G V, Pradeesh K, Kumar A, Kumar R, Rao S V, Markham M L and Baumberg J J 2008 *Mater. Lett.* **62** 1183
- [39] Bahae M S, Said A A, Wel T H, Hagen D J and Van Stryland E W 1990 *IEEE J. Quant. Electron.* **26** 760
- [40] Swain D, Anusha P T, Prashant T S, Tewari S P, Sarma T, Panda P K and Rao S V 2012 *Appl. Phys. Lett.* **100** 141109
- [41] Anusha P T, Reeta P S, Giribabu L, Tewari S P and Rao S V 2012 *Mater. Lett.* **64** 1915
- [42] Hamad S, Tewari S P, Giribabu L, Rao S V and Porphy J 2012 *Phth.* **16** 140
- [43] Saravanan K V, James Raju K C, Krishna M G, Tewari S P and Rao S V 2012 *Appl. Phys. Lett.* **96** 232905
- [44] Cullity B D 1957 *Elements of X-Ray Diffraction* (Reading, MA: Addison Wesley)
- [45] Jiang P, Zhou J J, Fang H F, Wang C Y, Wang Z L and Xie S S 2007 *Adv. Funct. Mater.* **17** 1303
- [46] Zhang W D 2006 *Nanotechnology* **17** 1036
- [47] Li H, Liang C, Zhong K, Liu M, Hope G A, Tong Y and Liu P 2009 *Nanoscale Res. Lett.* **4** 1183
- [48] Tauc J, Grigorovici R and Vancu A 1996 *Phys. Status Solidi b* **15** 627
- [49] Mott N F and Davis E A 1979 *Electronic Processes in Non-Crystalline Materials* 2nd edn (Oxford: Clarendon)
- [50] Vispute R D *et al* 1998 *Appl. Phys. Lett.* **73** 348
- [51] Cho S, Ma J, Kim Y, Sun Y, Wong G K L and Ketterson J B 1999 *Appl. Phys. Lett.* **75** 18
- [52] Meyer B K *et al* 2004 *Phys. Status Solidi b* **241** 231
- [53] Leiter F H, Alves H R and Hofstaetter A 2001 *Phys. Status Solidi b* **4** 226
- [54] Li Z, Xiong Y and Xie Y 2003 *Inorg. Chem.* **42** 8105
- [55] Lin B, Fu Z and Jia Y 2001 *Appl. Phys. Lett.* **79** 943
- [56] Jeong S-H, Kim B-S and Lee B-T 2003 *Appl. Phys. Lett.* **82** 2625
- [57] Kwok W M, Djurišić A B, Leung Y H, Chan W K and Phillips D L 2005 *Appl. Phys. Lett.* **87** 223111
- [58] Zhou J, Wang Y, Zhao F, Wang Y, Zhang Y and Yang L 2006 *J. Lumin.* **119-120** 248
- [59] Willander M, Nur O, Bano N and Sultana K 2009 *New J. Phys.* **11** 125020
- [60] Rajalakshmi M, Arora A K, Bendre B S and Mahamuni S 2000 *J. Appl. Phys.* **87** 2445
- [61] Damen T C, Porto S P S and Tell B 1966 *Phys. Rev.* **142** 570
- [62] Samanta K, Aroraand A K and Katiyar R S 2012 *J. Phys. D: Appl. Phys.* **45** 185304
- [63] Cusco R, Alarcon-Llado E, Artus L, Ibanez J, Jimenez J, Wang B and Callahan M J 2007 *Phys. Rev. B* **75** 165202
- [64] Serrano J, Romero A H, Manjo'n F J, Lauck R, Cardona M and Rubio A 2004 *Phys. Rev. B* **69** 094306
- [65] Exarhos G J and Sharma S K 1995 *Thin Solid Films* **27** 270
- [66] Xing Y J, Xi Z H, Xue Z Q, Zhang X D, Song J H, Wang R M, Xu J, Song Y, Zhang S L and Yu D P 2003 *Appl. Phys. Lett.* **83** 1689
- [67] Rao S V, Prashant T S, Sarma T, Panda P K, Swain D and Tewari S P 2011 *Chem. Phys. Lett.* **514** 98
- [68] Lin J-H, Chen Y-J, Lin H-Y and Hsieh W-F 2005 *J. Appl. Phys.* **97** 033526
- [69] Bazaru T, Vlad V I, Petris A and Miu M 2010 *J. Opt. Adv. Mat.* **12** 43
- [70] Lee H W, Anthony J K, Nguyen H-D, Mho S-I, Kim K, Lim H and Rotermund F 2009 *Opt. Express* **17** 19093
- [71] Zhang W, Wang H, Wong K S, Tang Z K, Wong G K L and Jain R 1999 *Appl. Phys. Lett.* **75** 3321
- [72] Divall M, Osvay K, Kurdi G, Divall E J, Klebniczki J, Bohus J, Péter Á and Polgár K 2005 *Appl. Phys. B* **81** 1123
- [73] Ganeev R A, Kulagin I A, Ryasnyanski A I, Tugushev İ R I and Usmanov T 2003 *Opt. Spectrosc.* **94** 561
- [74] Anusha P T, Swain D, Hamad S, Prashant T S, Giribabu L, Tewari S P and Rao S V 2012 *J. Phys. Chem. C* **116** 17828
- [75] Swain D, Rana A, Panda P K and Rao S V 2014 *Chem. Phys. Lett.* **610-611** 310